Applied Catalysis B: Environmental 182 (2016) 336–346

Contents lists available at ScienceDirect

Applied Catalysis B: Environmental

journal homepage: www.elsevier.com/locate/apcatb

Dual coke deactivation pathways during the catalytic cracking of raw bio-oil and vacuum gasoil in FCC conditions

Álvaro Ibarra[a], Antonio Veloso[b], Javier Bilbao[a], José Mª Arandes[a], Pedro Castaño[a,*]

[a] Chemical Engineering Department, University of the Basque Country (UPV/EHU), P. O. Box 644, 48080 Bilbao, Spain
[b] POLYMAT, University of the Basque Country (UPV/EHU), Joxe Mari Korta R&D Center, Avda. Tolosa-72, Donostia-San Sebastián 20018, Spain

ARTICLE INFO

Article history:
Received 15 July 2015
Received in revised form
10 September 2015
Accepted 18 September 2015
Available online 25 September 2015

Keywords:
Biomass pyrolysis
Bio-oil
Fluid catalytic cracking
Coke deactivation
HY zeolite

ABSTRACT

Coke deposition pathways have been studied during the fluid catalytic cracking of bio-oil, vacuum gasoil (VGO) and a blend of the previous two (80 wt% VGO and 20 wt% bio-oil), under realistic riser conditions of the fluid catalytic cracking (FCC) unit, using a commercial catalyst at 500 °C and contact times of 1.5–10 s. Amount and composition of soluble and insoluble coke in dichloromethane have been analyzed using a set of techniques (TPO, FTIR, ^{13}C NMR, XPS, Raman, GC–MS and MALDI-TOF MS, among others). The relationship of coke deposition with its composition and the reaction medium has allowed us to set two pathways of coke formation: (i) heavy hydrocarbon pathway tend to form ordered polycondensed aromatic nanostructures; whereas (ii) oxygenate pathway tend to form a lighter fraction of coke containing oxygen, less ordered and more aliphatic coke. A synergy between the two pathways have been verified due to the lower coke deposition of the blend compared to the individual components, and this has been explained in terms of (i) attenuation of the heavy hydrocarbon pathway caused by the steam contained or originated from the bio-oil, and (ii) the hydride transfer from hydrocarbons to the precursors of the oxygenate pathway.

1. Introduction

The increasing energy demand and restrictive environmental policies are contributing to the technological development of alternative routes of lignocellulosic biomass valorization, decreasing the dependency of fossil sources like natural gas, charcoal, shale or crude [1]. Bio-refinery concept pretend to use existing, revamped or new infrastructure of the refinery for producing at industrial scale platform chemicals and fuels from the products derived of several valorization routes of biomass: (i) fermentation, (ii) gasification, and (iii) flash pyrolysis, which respective intended products are bio-ethanol, synthesis gas and bio-oil (liquid product from pyrolysis). The selective production of bio-oil by flash pyrolysis has attracted a deep commercial and research interest [2–5], due to its features: low environmental impact, possibility of scale-up, and possibility of delocalizing pyrolysis units close to collection points, with a subsequent transport of the bio-oil to the refinery for large scale valorization [6].

Raw bio-oil [7–10] is a complex mixture of water (15–50 wt%) and oxygenates, and among them hydroxyl-aldehydes, hydroxyl-acetones, sugars, carboxylic acids and phenols. Moreover, raw bio-oil has a relatively low heating value (16–19 MJ kg^{-1}), low volatility, thermal and chemically unstable, corrosive (pH≈2–4 due to carboxylic acids) and highly viscous (10–100 cP at 40 °C). The main routes of raw bio-oil valorization are: (i) component extraction, (ii) use as a fuel or fuel-blending in combustion engines, (iii) steam reforming to produce H_2, (iv) catalytic transformation trough cracking or hydrodeoxygenation. Among them, catalytic cracking is peculiarly viable in terms of versatility, possibility of scaling up and value of the products obtained. In this sense, the fluid catalytic cracking (FCC) unit shows enhanced prospects for bio-oil upgrading due to the fact that has been designed for treating complex and heavy feeds [11].

Several works in literature have pointed to the high conversion of raw bio-oil in FCC conditions [12–15], together with a strong synergism between the cracking of hydrocarbons and oxygenates, affecting the composition and quality of products [16,17]. Indeed, the co-feeding of raw bio-oil with the standard feedstock of the FCC shows several uncertainties applied to the required modifications of the FCC unit: catalyst-oil contact times, design modifications, process conditions and catalyst deactivation. Coke deposition takes a key role in the energy and mass balance of the FCC unit that operates with a regenerator section, providing heat by coke com-

* Corresponding author.
E-mail address: pedro.castano@ehu.es (P. Castaño).

http://dx.doi.org/10.1016/j.apcatb.2015.09.044

bustion to the endothermic cracking reactions and also (in the same combustion) wasting carbon to produce CO_2.

Coke deposition has attracted great interest in the studies of bio-oil cracking [18–20], particularly using an HZSM-5 zeolite catalyst and different fractions of bio-oil or thermally-catalytically treated bio-oil. These treatments aim to remove the fraction of bio-oil that more easily condensates toward bio-char or thermal pyrolytic lignin, which at the same time has its own valorization routes [21]. Previous studies indicate that there are three important parameters, sometimes correlated, affecting the coke deposition and the corresponding catalyst deactivation [22,23]: (i) catalyst features, mainly the pore network topology, zeolite size and acidity; (ii) process conditions, largely influenced by temperature; and (iii) reactor medium, in terms of the presence of steam and certain oxygenates. Steam has a double influence for coke suppression: neutralizing the strongest acid sites (responsible of certain condensation reactions of coke precursors) and stripping coke precursors from the catalyst [24]. On the other hand, several studies point that there are two pathways of coke formation in the co-processing of hydrocarbons and oxygenates: the oxygenate pathway, forming polyphenols residue with more aliphatic and oxygenated nature [19,20] from aldol condensation [25]; and the hydrocarbon pathway, forming polycondensed aromatic structures in consecutive steps (commonly abbreviated as condensation) of alkylation, dehydrogenation and cyclation. Several studies on the cracking of bio-oils in fixed bed reactors support these pathways [26–28].

Attending to these considerations, in this work we have deepen in the effect of co-feeding bio-oil with vacuum gasoil on the mechanisms of coke formation over the catalyst in realistic FCC conditions. To this aim, fluid catalytic runs were performed using an equilibrated commercial catalyst in a riser simulator reactor targeting short contact times (1.5–3 s) and analyzing product distribution. The catalyst degradation and coke nature were analyzed and correlated with process conditions, composition of the reactor medium and catalytic features to obtain a picture of the deactivation pathways. The degradation of the catalysts was assessed comparing the properties of the fresh and spent samples. The composition of coke was obtained using a set of different spectroscopic and thermogravimetrical techniques on the spent catalyst, the soluble or insoluble coke in dichloromethane: thermogravimetrical temperature programmed oxidation (TG-TPO), Fourier transformed infrared (FTIR) spectroscopy, ^{13}C coupled polarized magic angle spinning nuclear magnetic resonance (CP-MAS NMR), X-ray photo spectroscopy (XPS), Raman spectroscopy, gas chromatography with mass spectrometry detector (GC–MS) and matrix assisted laser desorption ionization time of flight mass spectrometry (MALDI-TOF MS).

2. Experimental

2.1. Feed properties

Three feeds have been used: vacuum gasoil (VGO), raw bio-oil (RBO) and the mixture of VGO (80 wt%) with bio-oil (20 wt%), named MIX. The RBO has been obtained by fast pyrolysis of black poplar sawdust at 440–450 °C in a N_2 stream, using a pilot plant provided with a conical spouted bed reactor [29]. The feeds have been characterized by simulated distillation (following the norm ASTM D2887 in an Agilent 6890 Series GC System with a column Simdis D2887 Fast/Ext.) and elemental analysis (LECO TruSpec CHN Macro). The concentrations of the component families in the RBO have been determined by GC–MS (Shimadzu GC–MS QP2010, BPX5 column of 50 m × 0.22 mm × 0.25 μm). The water content was measured by Karl-Fisher method (Metrohm 830KF Titrino plus). The properties of the feeds are detailed in the Tables 1 and 2 for the RBO and VGO, respectively.

Table 1
Composition of the raw bio-oil (RBO).

Elemental composition (wt%)	
C	29.4
H	8.5
S	0.4
O	61.7
Water content (wt%)	46.0
Composition in dry basis (wt%)	
Acetic acid	15.5
Other acids and esters	6.2
Hydroxy-acetaldehyde	7.8
Other aldehydes	11.6
1-Hydroxy-2-propanone	6.5
Ketones	9.8
Phenols	5.1
Alcohols	9.7
Ethers	2.8
Levoglucosan	21.6
Others	2.5
Non identified	0.9
Simulated distillation (°C), D2887	
Initial boiling point	35
5 wt%	55
25 wt%	74
50 wt%	154
90 wt%	263
Final boiling point	335

Table 2
Composition of the vacuum gas oil (VGO).

Density (g cm^{-3})	0.918
Average molecular weight (g mol^{-1})	370.3
Elemental composition (wt%)	
C	85.4
H	11.8
S	2.8
O	–
Composition (wt%)	
Aliphatics	47.2
Aromatics	43.1
Sulfur compounds	9.7
Simulated distillation (°C), D2887	
Initial boiling point	184
5 wt%	367
25 wt%	432
50 wt%	474
90 wt%	533
Final boiling point	614

2.2. Catalyst characterization

An equilibrated industrial FCC catalyst containing 15 wt% HY zeolite has been used. The physical properties and porous structure have been determined by N_2 adsorption–desorption (Micromeritics ASAP 2010) and the crystal structure by X-ray diffraction using the sample as a powder (Phillips PW1710, using a radiation of Cu Kα). The acidity and acid strength have been obtained by the isothermal adsorption of NH_3 at 150 °C. Subsequently, temperature programmed desorption (TPD) of absorbed NH_3 has been carried out following a ramp of 5 °C min^{-1} up to 550 °C (thermobalance, TA Instruments SDT 2960, online with a mass spectrometer, MS Thermostar Balzers Instruments). The Brönsted/Lewis ratio has been determined by FTIR spectrophotometry with pyridine adsorbed (Thermo Nicolet 6700). Table 3 summarizes the main catalyst properties.

Table 3
Properties of the commercial equilibrated catalyst.

Physical properties	
S_{BET} ($m^2\,g^{-1}$)	122
V_p ($cm^3\,g^{-1}$)	0.15
d_p (Å)	117.3
Unit cell size (Å)	24.3
Acid properties	
Zeolite percentage (wt%)	15
Total acidity ($\mu mol\,g^{-1}$)	30
Average acid strength ($kJ\,mol^{-1}$)	100
Brönsted/Lewis ($mol\,mol^{-1}$)	0.75

2.3. Reaction equipment and product analysis

The reaction runs have been carried out in a riser simulator reactor described before [30]: This is an internal recycle reactor where the catalyst is fluidized continuously (during the reaction run) with an internal impeller for thrusting the gas (feed and products) throughout the catalyst bed. The riser simulator is ideal for simulating the conditions employed in the industrial FCC units, particularly in terms of reaction time and fluidization. The reactions were performed at 500 °C; time, 1.5–10 s; catalyst/feed mass ratio in dry base, 6 g_{cat} $(g_{feed})^{-1}$ for the VGO and MIX cracking and 7.6 g_{cat} $(g_{feed})^{-1}$ for the RBO cracking. The product stream has been analysed after the required time, by gas chromatography (Agilent Technologies 7890 A, with FID and PFPD detectors) and by gas micro chromatography (Varian CP-4900) to quantify CO and CO_2). The products have been grouped according to the typical FCC procedure accounting the existence of extra products coming from the presence of oxygenate fraction: CO, CO_2, dry gases (C_1–C_2), liquefied petroleum gases (LPG, C_3–C_4), gasoline (C_5–C_{12}), light cycle oil (LCO, C_{13}–C_{20}), heavy cycle oil (HCO, C_{20+}) and coke. The amount of coke has been determined using the mass loss of spent catalyst after combustion in a thermobalance (TGA-Q 5000 TA Instruments) by following a heating rate of 3 °C min^{-1} from 300 °C up to 550 °C. The conversion of the VGO, RBO or the MIX has been obtained by the sum of dry gas, LPG, gasoline and coke, which is a standard criteria in FCC units:

$$X = Y_{drygas} + Y_{LPG} + Y_{gasoline} + Y_{coke} \quad (1)$$

where the yields of each lump (Y_i) have been defined as the weight produced of this specific lump (m_i) divided by the weight of the feed in dry basis ($m - m_{water}$):

$$Y_i = m_i(m - m_{water})^{-1} \times 100 \quad (2)$$

2.4. Coke characterization

The spent catalysts have been analysed using a set of techniques already used in previous studies to discern composition and location of the coke derived from the reactions involved [19,20].

Temperature programmed oxidation (TPO) was followed by FTIR spectroscopy (Thermo Nicolet 6700) in a catalytic transmission cell (Specac HPHT) and with on-line gas analysis using a mass spectrometer (MS, Pfeiffer Vacuum GSD 320 O2) to follow the CO_2 produced during the combustion (m/z = 44 uma). The pelletized sample was set to vacuum conditions at 100 °C to desorb water and remove impurities. Then, 50 mL min^{-1} are allowed to pass through the catalytic chamber, a background spectrum is performed and subsequent temperature rising up to 450 °C at 5 °C min^{-1}, keeping this final temperature for 60 min and recording throughout the TPO the FTIR and MS spectra.

The spent catalysts were analyzed by ^{13}C CP-MAS NMR, using a probe of 7 mm and rotating it at 10 kHz. The pulse sequence was carried out in a Bruker DXR 400 WB PLUS 9.40T, using a frequency of 79.5 MHz and spectral width of 30 kHz. The data acquisition and processing was performed with the TOPSPIN 1.3 (Bruker) software.

Raman spectroscopy has been performed in a Renishaw confocal microscope using a laser excitation source of 514 nm, subtracting the fluorescence effect of the deactivating species.

The spent catalysts were subjected to HF (Merck, 40 wt% in water) in order to obtain a soluble (*S*) coke fraction in dichloromethane (CH_2Cl_2, Panreac, 98 % purity) and an insoluble (*I*) coke fraction. The method involves grinding 100–400 mg of the spent catalyst, digesting in HF and extracting *S* coke using CH_2Cl_2. *S* coke has been analyzed using a GC–MS (Shimadzu QP2010) and *I* coke fraction was analyzed by Raman, XPS and MALDI-TOF MS techniques as discussed below.

XPS was performed in a SPECS system equipped with a Phoibos analyzer 150 1D-DLD and source of Al Kα monochromatic radiation. MALDI-TOF MS measurements were performed on a Bruker Autoflex Speed instrument (Bruker, Germany) equipped with a 355 nm Nd:YAG laser. All spectra were acquired in the positive-ion reflectron mode (accelerating voltage 20 kV, pressure 5×10^{-6} mbar). Each sample was dissolved in THF at 10 g L^{-1}, prepared according to the "dry droplet" method using two different types of sample targets: polished steel and PAC™ II (Pre-spotted AnchorChip), which is a pre-spotted α-cyano-4-hydroxy cinnamic acid (HCCA) matrix. For the first case, Dithranol was used such as MALDI matrix dissolved at concentration of 20 g L^{-1} in THF [31]. The matrix and sample solutions were premixed in the ratio 1:1.

3. Results

3.1. Coke selectivity

Fig. 1 shows the results of the conversion evolution with reaction time in the cracking of the three feeds (VGO, RBO and MIX) (Fig. 1a) and the selectivity of coke of the same data points according to the observed conversion (Fig. 1b). Coke selectivity has been calculated from the yields (quantified using TG-TPO results) and the feed conversion. In Fig. 1b different lines have been drawn corresponding to particular yields of coke. Fig. 1a shows that conversion of RBO is higher than that of VGO, and that the conversion of the MIX is higher than that predicted by the weighted arithmetic mean of the corresponding RBO and VGO. These results are attributed to the synergetic effect between the RBO and VGO conversions on zeolites, which have been explained in the literature according to two phenomena: (i) hydride transfer from hydrocarbons to oxygenates [27,32–34], and (ii) competitive adsorption of the hydrocarbons and oxygenates, stronger for the first ones, by the acid sites of the catalyst [35,36]. Interestingly, at contact times of about 1.5 s the conversion is already reaching the value of steady state, reached after 3 s (Fig. 1a), being coke an almost primary product and whose selectivity decreases for higher conversion values and contact times (Fig. 1b). The MIX blend has the lowest coke selectivity among the feeds employed, which can be attributed to two combined effects: (i) the attenuating effect of steam contained in the bio-oil on the coke formation from the hydrocarbons of VGO [37], (ii) the hydride transfer from paraffinic compounds in VGO to oxygenates in bio-oil [38,39] enabling a lower deposition of coke. On the other hand, RBO cracking has the highest selectivity of coke although with the highest final conversion, indicating that coke deposited does not affect acid sites as much as the coke deposited on the cracking of VGO.

Fig. 2a shows the effect of coke deposition on the product distribution of the cracking of the three feeds, for a reaction time of 6 s. The product distribution within the gasoline fraction (Fig. 2b) shows that the cracking of VGO yields a product rich in aromatics, olefins, *i*-paraffins, naphthenics and *n*-paraffins. The cracking

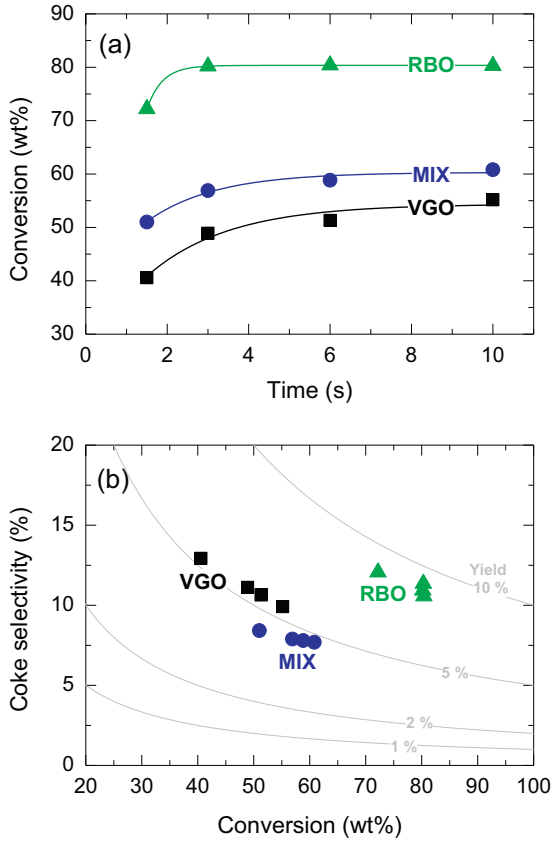

Fig. 1. Evolution with reaction time of conversion (a) and evolution with the conversion of coke selectivity (b) in the cracking of the feeds. Yield (grey) lines of Fig. 1b have been calculated assuming that Y_{coke} = (coke selectivity) × (conversion).

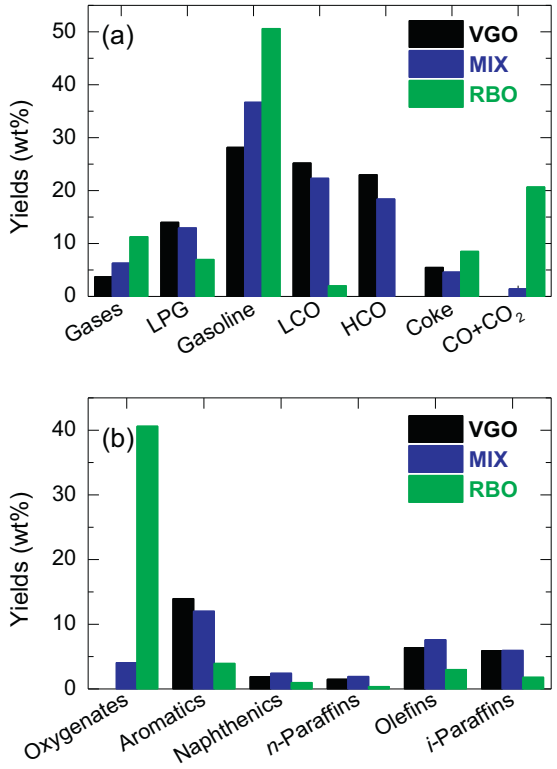

Fig. 2. Yields of product fractions in the cracking of the feeds at 6 s (a) and yields of gasoline fraction in the cracking of the feeds at 6 s (b).

Table 4
Properties of the fresh and spent catalyst used in the cracking of the feeds.

Catalyst	S_{BET} ($m^2\ g^{-1}$)	V_{mp} ($cm^3\ g^{-1}$)	V_p ($cm^3\ g^{-1}$)
Fresh	122	0.042	0.154
Spent (VGO, 1.5 s)	93	0.029	0.184
Spent (VGO, 3 s)	79	0.025	0.141
Spent (MIX, 1.5 s)	91	0.029	0.177
Spent (MIX, 3 s)	85	0.027	0.175
Spent (RBO, 1.5 s)	82	0.024	0.187
Spent (RBO, 3 s)	80	0.025	0.173

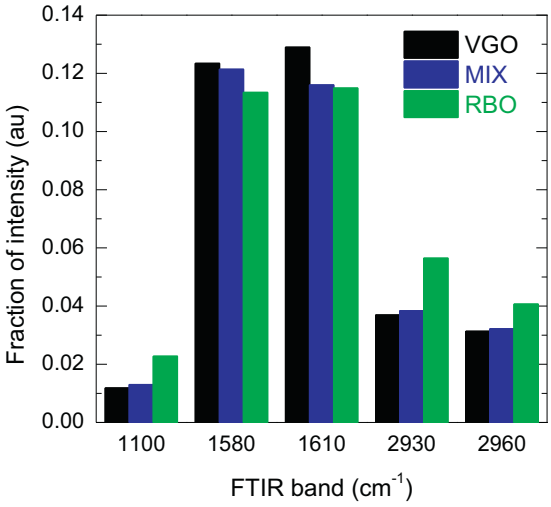

Fig. 3. Fraction of FTIR intensity bands associated with the coke deposited on the catalyst used in the cracking of the feeds at 6 s.

of MIX produces intermediate yields of products but significantly lower yields of oxygenates in gasoline and CO + CO_2 than the values predicted from the composition of MIX (20 wt% of RBO). This result indicates the hydride transfer from hydrocarbons to oxygenates, which favors the deoxygenation by formation of H_2O compared with the decarbonylation and decarboxylation reactions. Moreover, the lower coke deposition favors a higher yield of hydrocarbons in gasoline, with higher yields of naphthenics, *n*-paraffins and olefins compared to the one obtained with the individual components of MIX.

3.2. Catalyst deterioration

Table 4 summarizes the properties of the fresh and spent catalysts under different reaction times and feeds. Pores are considerably blocked due to coke deposition, particularly micropores. After 3 s, BET surface area decreases 35.2, 30.3 and 34.3% for the VGO, MIX and RBO spent catalysts, respectively. Once more, this observation proved that the coke deposited on the cracking of RBO induced less deterioration to the catalyst even considering the much higher yield of coke, than that of the cracking of VGO. The deterioration of the surface properties is very significant for contact times as low as 1.5 s in terms of BET surface area and micropore volume, with average drops of 25.4 and 31.0%, respectively.

3.3. Properties of the coke

3.3.1. FTIR spectroscopy

Fig. 3 shows the FTIR band intensities associated to the following coke functionalities [40,41]: 1100 cm^{-1}, aliphatic ethers or carboxylic acids; 1580 cm^{-1}, condensed aromatics also known as coke band; 1610 cm^{-1}, dienes and conjugated double bounds in coke; 2930 cm^{-1}, linear CH_2 and branched CH aliphatics; 2960 cm^{-1},

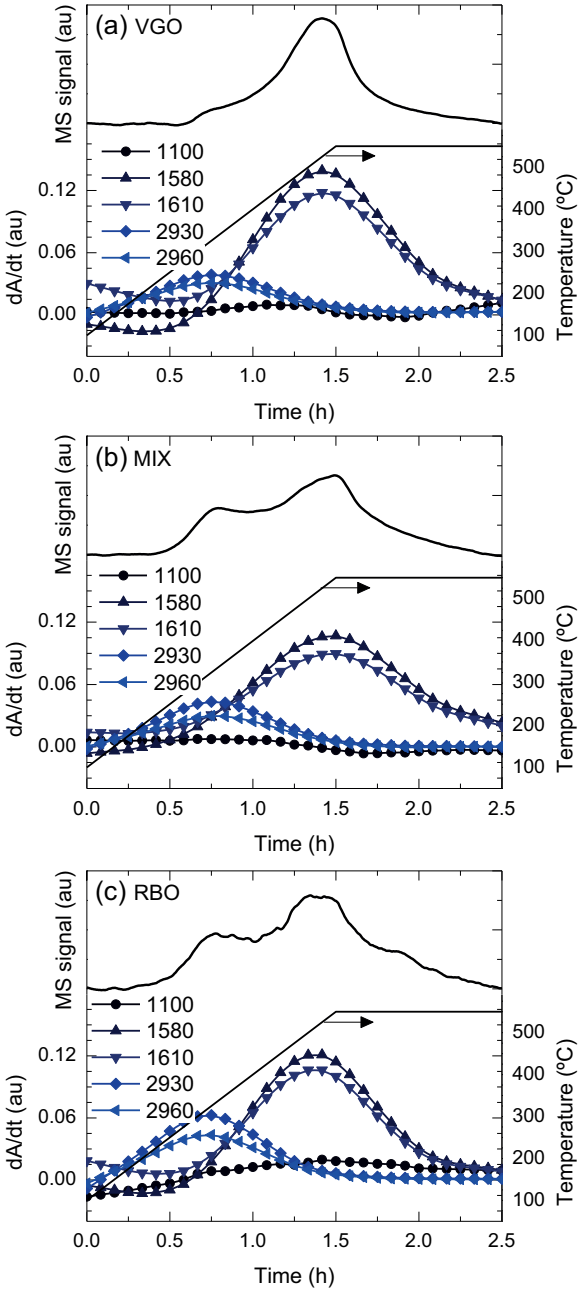

Fig. 4. TPO-MS and TPO-FTIR profiles of the coke deposited on the catalyst used in the cracking of the feeds: VGO (a), MIX (b) and RBO (c).

terminal CH_3 aliphatics. The 1100 cm^{-1} band could not be univocally associated with aliphatic ethers or carboxylic acids but seems a plausible association. Coke deposited on the VGO spent catalyst contains more condensed aromatics and dienes, whereas that on the RBO spent catalyst contains more aliphatics and oxygenates. Coke deposited on the MIX spent catalyst has intermediate composition between that of VGO and RBO spent catalysts.

3.3.2. TPO-FTIR/MS analysis

Fig. 4 shows the TPO profiles of the coke deposited on the spent catalysts using two techniques: CO_2 mass spectrometry (MS) signal in the upper part and FTIR spectroscopy in the lower part of each axis. The MS profiles are qualitatively similar for the three feeds, with two combustion peaks, at 300 and 500 °C. According to the change of the FTIR bands, the first combustion peak at 300 °C coincides with the removal of aliphatics and with the initiation of aromatic and diene combustion, thus associating this peak with hydrogenated coke with relatively high H/C ratio, or with a low-developed coke placed in the exterior of the microporous crystals of the catalyst [42]. On the other hand, the combustion peak at 500 °C is related with the combustion of high-developed coke consisting both in condensed aromatics and dienes, originated in the micropores of the catalyst but developed outside (assumable due to its high condensation) with the occurrence of reactions as cyclations, aromatizations, and condensations that are catalyzed by internal or external acidity [23].

The coke deposited on the VGO spent catalyst (Fig. 4a) contains higher proportion of the second combustion peak at 500 °C, and more intense aromatic and diene bands. On the other hand, the coke deposited on the RBO spent cracking (Fig. 4c) contains higher fraction of the first combustion peak at 300 °C. These results are in line with the previous FTIR profiles shown in Fig. 4 and others shown in the literature [22,43], that demonstrate the graphitic nature of coke deposited upon the FCC operation, favored by the harsh conditions used in the unit and the relatively high molecular weight of the feedstock (VGO) with condensed aromatics already present in the composition. The deposited coke on the RBO spent catalyst (Fig. 4c) is more heterogenic by means of a significant concentration of aliphatics, oxygenates, polyaromatics and dienes, and broader combustion FTIR and MS peaks. This result coincides with these published before in the transformation of bio-oil to olefins using HZSM-5 zeolite catalyst [19,20], where the first combustion band is associated with the presence of coke with a thermal origin, from the polymerization of polyphenols [21], associated with amorphous and oxygenated coke having a lower apparent activation energy of combustion. Besides, the second peak combustion occurs at lower temperatures for the spent RBO catalyst compared to that of VGO spent catalyst, indicating the lower condensation of the former and the possible presence of oxygen within the structure.

The coke deposited on the MIX spent catalyst has a profile midway between the VGO and RBO, with an important contribution of the first combustion peak. Moreover, the temperature of the second combustion peak is 2 °C lower than that of the coke corresponding to VGO spent catalyst, what has been previously proved by Gueudré et al. [28]. The FTIR results presented in Fig. 4 demonstrate that the combustion of coke occurs with two parallel mechanisms: (i) selective combustion of the components of heterogeneous coke, with parallel (ii) degradation or aging of coke suffering dehydrogenation [44,45], and observed by the aliphatic behavior at temperatures lower than 250 °C, with negligible CO_2 formation, degradation of the aliphatic bands (2930 and 2960 cm^{-1}) and formation of the aromatic band (1580 cm^{-1}).

3.3.3. ^{13}CP-MAS NMR spectroscopy

^{13}C CP-MAS NMR spectra of spent catalysts are shown in Fig. 5. For the three feeds, two main bands are observed [46]; at 129 ppm assigned to aromatic C-nuclei, and a second one at *ca.* 20 ppm assigned to aliphatic terminal C-nuclei (CH_3). Moreover, two additional shoulders are observed at 141 and 29 ppm corresponding to condensed aromatic structures and linear (CH_2) or branched (CH) aliphatics. Attending to the ratio of aromatic:aliphatic it can be concluded that independently of the feed used, coke has a significant aromatic nature.

3.3.4. Raman spectroscopy

Fig. 6 shows the Raman spectra of the spent catalyst used in the cracking of the VGO, MIX or RBO. The spectra have been deconvoluted into 5 bands with the following average Raman shift and assignments [40,47,48]: 1213 cm^{-1}, ν_{C-H} band assigned to aliphatic bounds; 1383 cm^{-1}, *D* band assigned to aromatic structures poorly structured or disordered, 1496 cm^{-1}, D_3 band assigned to structural

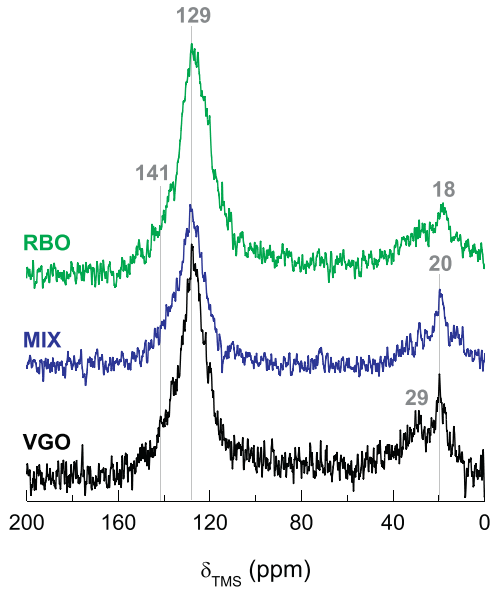

Fig. 5. ^{13}C CP-MAS NMR spectra of the coke deposited on the spent catalyst used in the cracking of the feeds at 6 s.

Table 5
Intensities of the Raman bands corresponding to the coke deposited on different spent catalysts used in the cracking of the feeds.

Feed	ν_{C-H}	D	D_3	G	D_2	D/G	$w{:}h$ (G)
VGO	0.133	0.313	0.008	0.359	0.186	0.872	0.119
MIX	0.143	0.366	0.069	0.271	0.151	1.352	0.234
RBO	0.170	0.369	0.097	0.246	0.118	1.499	0.243

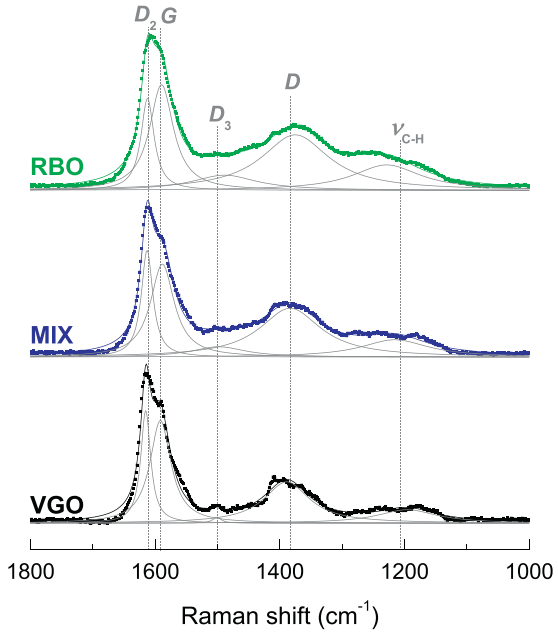

Fig. 6. Raman spectra of the coke deposited on the spent catalyst used in the cracking of the feeds at 6 s.

defects of aromatic domains with poor organization; 1590 cm^{-1}, G band assigned to more developed or structured aromatic clusters; and 1613–cm^{-1}, D_2 band which is also D echo band. The results of the 5 bands deconvolution of the Raman spectra are summarized in Table 5, together with the D/G ratio and the width to height ratio ($w{:}h$) of the G band. The fractions of ν_{C-H}, D and D_3 bands increase with the proportion of RBO fed to the reactor, whereas the fractions of G and D_2 bands have an opposing trend. Thus, indicating the higher ordering and lower amount of distortions and aliphatics in the coke deposited in the cracking of VGO as compared to that of RBO. The size of coke clusters is inversely related with the $w{:}h$ ratio [49] so that this size value is higher for the coke deposited on the VGO spent catalyst than that on the RBO spent catalyst. Besides, the D/G ratio values have the same trend pointing in the same higher ordering and size of coke clusters deposited during the cracking of VGO.

The combined results presented so far demonstrate that the coke deposited on the VGO spent catalyst has more aromatic and less oxygenated-aliphatic nature, with a relatively bigger and more ordered coke clusters, as compared with the coke deposited on the RBO spent catalyst. Moreover, the experimental conditions, similar to those of the FCC unit (with temperatures of about 500 °C in a transport bed with high velocity of gases), facilitate the decarboxylation, decarbonylation and dehydrogenation, homogenizing the composition of coke towards more condensed aromatic structures. To understand better the composition of coke and its impact on deactivation, we have extracted the soluble coke from the spent catalysts, analyzing the composition of soluble and insoluble coke separately.

3.4. Composition of soluble coke

The extraction of coke is a well known procedure to remove the catalyst structure (zeolite and matrix) in order to obtain a fraction soluble in CH_2Cl_2 known as S coke and a precipitated organic fraction known as I coke [50]. In FCC conditions, the S coke can be considered as trapped within the microporous structure of the spent catalyst, whereas the I coke (constituted by polyaromatics) is deposited within the matrix, having meso and macropores, of the catalytic particles [22]. Table 6 summarizes the content of the most important components of the S coke deposited on the VGO, MIX or RBO spent catalysts. These fractions have been grouped into the following families: A_{1-4}, aromatics of 1 up to 4 rings; O, linear oxygenates; and O_{1-2}, oxygenates with 1 up to 2 aromatic, naphthenic or oxo-naphthenic ring. There is a significant difference in the amount of S and I coke deposited on the spent catalysts, with much higher content of S coke for the RBO spent catalyst and with higher content of I coke for the VGO spent catalyst, being the MIX spent catalyst midway between the two. The relatively light composition of coke (corresponding to a lower I/S ratio) deposited on the RBO spent catalyst offers good perspectives for being eliminated with the steam on the stripping of the FCC unit. Table 6 also shows significant differences within the composition of S coke for the different feeds: VGO promotes the existence of aromatics in the S coke, particularly methylnaphthalenes (A_2), whereas for the RBO a bimodal distribution is observed with a hydrocarbon pool (28 wt%) with relatively heavier fractions of these of S coke deposited on VGO spent catalyst and an additional oxygenate pool (72 wt%) with mainly O_1 molecules. Once more, MIX spent catalyst shows halfway composition of its S coke between these of VGO and RBO spent catalysts.

Interestingly, the total amount of coke deposited on the MIX spent catalyst is lower than that of the separated components of the mixture, what coincides with the lowest deterioration of the catalyst properties shown in Table 4 (after 3 s). This attenuation occurs mainly on the I coke content side. Considering the facts that VGO promotes the I coke deposition whereas RBO facilitates the deposition of S coke one, a logical interpretation is that the steam present in RBO (not present in the VGO) inhibits the deposition of the I coke from the VGO fraction.

Table 6
Content of total, soluble (*S*) and insoluble (*I*) coke deposited on the spent catalysts used in the cracking of the feeds. A_1, one ring aromatics. A_2, two ring aromatics. A_3, three ring aromatics. A_4, four ring aromatics. *O*, alkyl oxygenates. O_1, one ring oxygenates. O_2, two ring oxygenates of the *S* coke.

	VGO	MIX	RBO	Main components
Coke (wt%)	0.91	0.70	1.12	
S coke (wt%)	0.14	0.18	0.58	
I coke (wt%)	0.77	0.52	0.54	
I/*S* ratio	5.50	2.89	0.93	
A_1 (wt%)	17	14	0	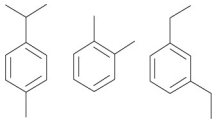
A_2 (wt%)	76	37	16	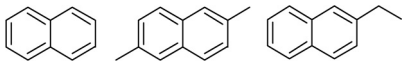
A_3 (wt%)	7	7	7	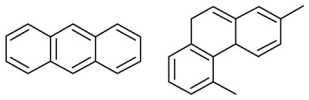
A_4 (wt%)	0	3	5	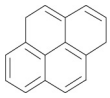
O (wt%)	0	18	25	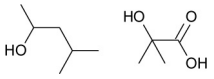
O_1 (wt%)	0	17	38	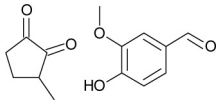
O_2 (wt%)	0	4	9	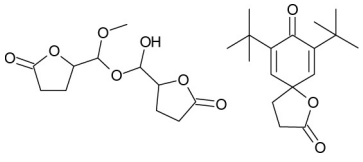

Table 7
Intensities of the Raman bands corresponding to the insoluble coke deposited on different spent catalysts used in the cracking of the feeds.

Feed	ν_{C-H}	*D*	D_3	*G*	D_2	*D*/*G*	*w*:*h* (*G*)
VGO	0.163	0.381	0.057	0.181	0.218	2.100	0.155
MIX	0.145	0.395	0.035	0.178	0.246	2.216	0.158
RBO	0.202	0.405	0.140	0.147	0.250	2.737	0.219

3.5. Composition of insoluble coke

I coke is associated to more developed or graphitic type of carbonaceous residue, whose location lays on the meso and macropores of the FCC catalytic matrix. In this sense, we have analyzed *I* coke by means of combined Raman, XPS spectroscopies and MALDI-TOF spectrometry.

3.5.1. Raman spectroscopy

Fig. 7 shows the Raman spectra of the *I* coke deposited on the spent catalysts and the deconvolutions in different bands, which have been summarized in Table 7. In this case, the same bands observed for the total coke in Fig. 6 appear at different average Raman shift values: 1251 cm^{-1}, ν_{C-H} band; 1374 cm^{-1}, *D* band, 1493 cm^{-1}, D_3 band; 1577 cm^{-1}, *G* band; and 1613 cm^{-1}, D_2 band. These changes indicate that with the exception of the ν_{C-H} band, for the *I* coke all the bands move towards lower Raman shift values. This observation, together with the higher values of *D*/*G* ratio (Tables 5 and 7), is an indication that *I* coke is more developed

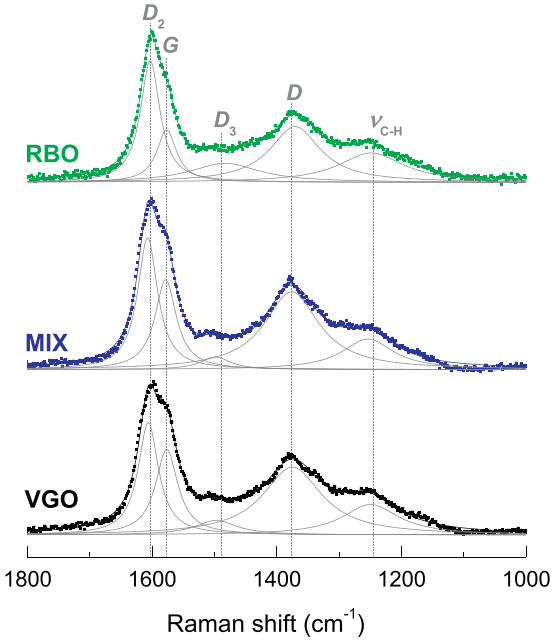

Fig. 7. Raman spectra of the insoluble coke deposited on the spent catalyst used in the cracking of the feeds at 6 s.

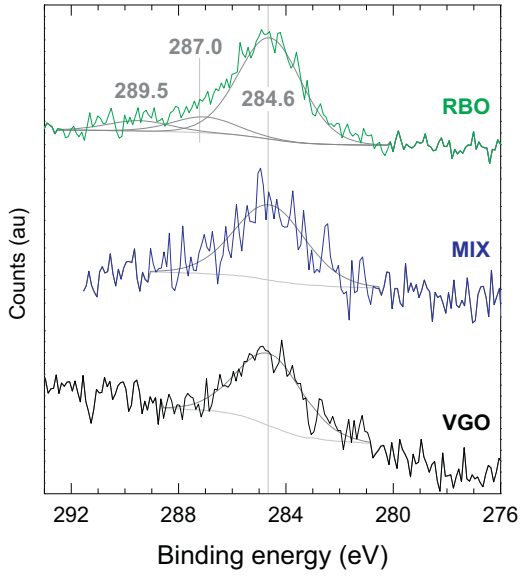

Fig. 8. XPS spectra of the insoluble coke deposited on the spent catalyst used in the cracking of the feeds at 6 s.

or ordered. Besides, Table 7 shows that the bands for the *I* coke deposited during the cracking of VGO corresponds to a higher ordering and lower amount of distortions and aliphatics than that of the *I* coke deposited during the cracking of RBO.

3.5.2. XPS spectroscopy

XPS spectra displayed on Fig. 8 show the C band of the *I* coke corresponding to the different feeds. All spectra show a more intense band at 284.6 eV assigned to C bounded with other C or H. The two shoulders appearing for the *I* coke deposited on the RBO spent catalyst at 287.0 and 289.5 eV correspond to C bounded with O [21], indicating that oxygen takes place in the composition of this *I* coke but does not in that of the MIX spent catalyst. In other words, *I* coke deposited on the MIX spent catalyst is closer to that on the VGO spent catalyst in terms of composition.

3.5.3. MALDI-TOF mass spectrometry

MALDI spectra of the *I* coke using dithranol, such as matrix, is shown in Fig. 9. These spectra represent the crackdown pattern of the *I* coke deposited on the spent catalysts. *I* coke deposited on the RBO spent catalyst shows a narrower mass distribution, centered in weights of about 602 uma, whereas the profiles of *I* coke deposited on the MIX and VGO stent catalysts are relatively similar among them; having a maxima at lower weights (575 uma) but a distribution moved towards higher values of weight. Fig. 10 in the supporting information shows the distribution of weights of the *I* coke, summing the counts in 18 intervals for better visualization. Indeed, the *I* coke deposited on the MIX and VGO spent catalyst are centered in 760 uma. These values of the mean *I* coke weights are relatively larger than, for example, that of coke deposited on the ethanol cracking at 350 °C [51], or on a FCC industrial spent catalyst (after the stripper and with steam present in the riser) [43] and much larger compared to the one deposited on the isobutene/butene alkylation at 130 °C [52]. On the other hand, these values are comparable to these obtained with coke deposited on the cracking of *n*-butene at 500 °C [31].

Fig. 11 shows a detailed crackdown pattern in the range 560–640 uma for characterizing better the area surrounding the maximum count values. *I* coke deposited on the RBO spent catalyst shows a higher proportion of fractions divided by 1 uma (visualized like more noise) accounting a more hydrogenated nature of this

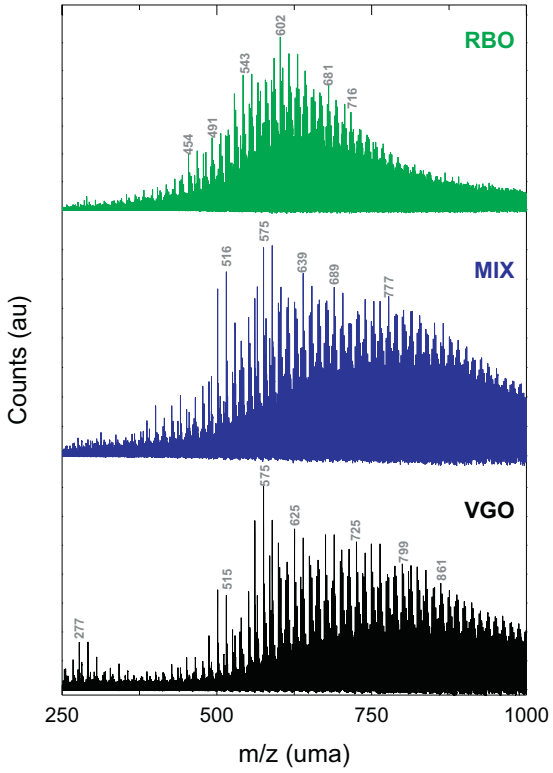

Fig. 9. MALDI-TOF spectra of the insoluble coke deposited on the spent catalyst used in the cracking of the feeds at 6 s.

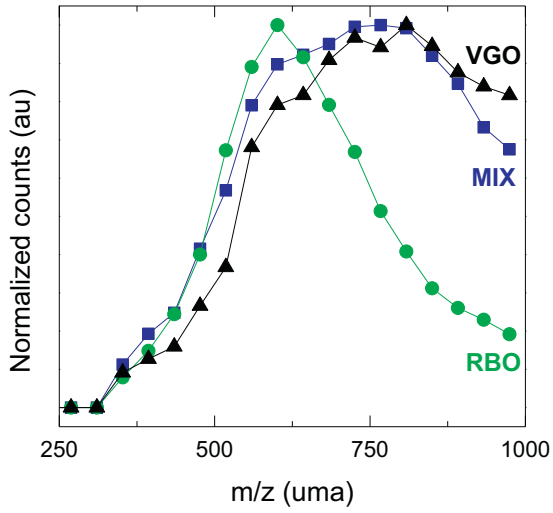

Fig. 10. Normalized distribution of the MALDI-TOF mass profiles.

coke, in agreement with these of FTIR spectroscopy for the total coke shown in Fig. 3. On the other hand, *I* coke deposited on the VGO spent catalyst is much less hydrogenated and shows much clear patterns divided by 14 uma (arrows in Fig. 11) corresponding to CH_2 aliphatic groups attached to aromatics (likewise in the MIX spent catalyst) [51]. The possible inclusion of oxygen within the *I* coke deposited on the RBO spent catalyst (as demonstrated in Fig. 8) and possible traces in that deposited on the MIX spent prevented us from proposing structures from *I* coke, as other authors have proposed for lighter coke without oxygen [51]. Nonetheless and as for give an idea of possible structures comprised in the *I* coke deposited on the spent catalyst, Fig. 12 shows some of these tentative structures.

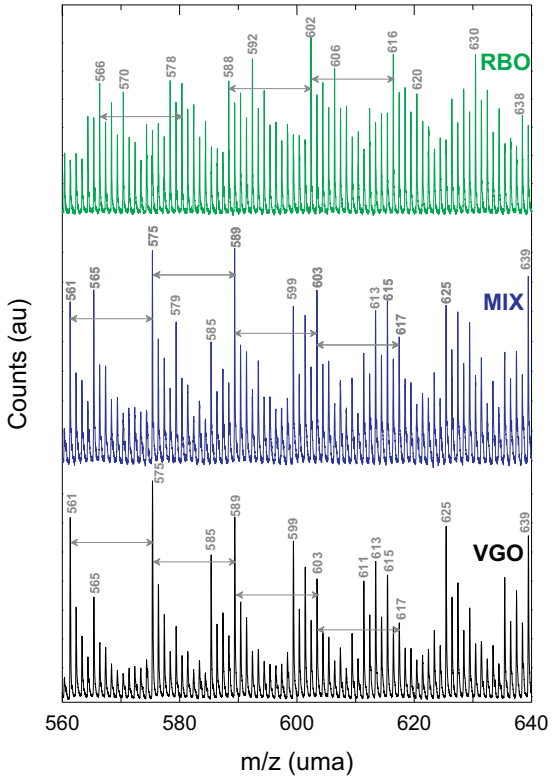

Fig. 11. Detail of the MALDI-TOF spectra corresponding to range 560–640 uma, of the insoluble coke deposited on the spent catalyst used in the cracking of the feeds at 6 s. The arrow indicates a difference of 14 uma.

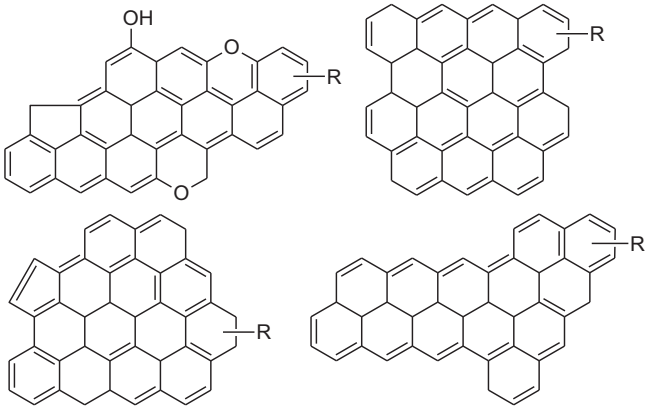

Fig. 12. Tentative structures implicated in the composition of insoluble coke.

4. Discussion

The results shown here point to the existence of two significantly different pathways of deactivation during the cracking of heavy hydrocarbons (as VGO) and oxygenates (as RBO). Coke deposited on the cracking of VGO is highly condensed, graphitic, mainly insoluble in CH_2Cl_2 and with a very high content of polyaromatics, in agreement with previous observations [22]. Polyaromatics are refractory molecules trapped within the meso and macropores of the catalytic matrix, blocking the accessibility to the acid sites, and developing towards higher condensation. The origin of the heavy aromatic coke formed during the cracking of VGO is an additive coke (or Conradson carbon) [22], deposited from the heavier HCO fraction of the feed, and it is formed within contact times lower than 1 s, i.e., inlet of the riser [53].

Coke deposited on the cracking of the RBO is relatively less condensed, lighter, more aliphatic and oxygenated respect to that deposited on the cracking of VGO. Coke precursors in the RBO are chemically different from these of the VGO. Nevertheless, the harsh conditions employed in the FCC unit enable to evolve the coke in a way that homogenize its composition, independently of the pathway taken, towards the formation of graphitic aromatic nanostructures on the meso and macropores of the catalyst, with compositional differences according to the feed used. In the cracking of RBO much more soluble coke is formed, 72 wt% of which are oxygenates and 28 wt% are aromatic hydrocarbons. Moreover, insoluble coke is lighter, less aggregated and posses C—O bounds in the structure. As it happens again, meso and macropores of the catalytic matrix are useful for acting as deposit-places of insoluble coke. Soluble coke seems to play a less important role in catalytic deactivation as the steady conversion (after 1.5 s) of RBO is very high, but when the reactions stops is an apparent deteriorating agent of the catalyst. Coke deposited on the RBO spent catalyst has higher H/C ratio (0.29) compared to VGO (0.14), and could be interpreted in some cases as the explanation of a lower deactivation caused by the bio-oil [54]. However, our results point to the higher deposition of coke due to the presence of oxygenates [33,55].

On the other side, the coke content of the RBO spent catalyst (1.12 wt%) is higher than that for the cracking of VGO (0.91 wt%) (Table 6), what is tolerable for the regeneration section of the FCC [56–58]. Coke deposited on the mixture blend (MIX) is in terms of composition halfway between these of the pure feeds (VGO and RBO) with higher similarity to that of VGO due to the higher proportion of it in MIX (80 wt%). The amount and composition of soluble coke formed with MIX is also predictable accounting its constituents. The composition of insoluble coke deposited in the cracking of MIX is similar to that of the VGO but its amount is lower, what we have explained in terms of the presence of steam from the RBO (containing 46 wt% of water). Steam acts as an inhibitor of insoluble coke formation due to the stripping effect of coke precursors and the competitive adsorption of steam and hydrocarbons on the acid sites, attenuating condensation reactions. The stripping is favored in the commercial FCC catalyst, with a hierarchical pore structure where the agglomerated HY zeolite contributes with micropores and the matrix (binder and filler) material contributes with meso and macropores. The matrix material provides with several benefits and in terms of deactivation it only retains the less volatile coke fraction (*I* coke) and enables coke precursors to escape from the catalytic pore system. During the cracking of MIX, both pathways of coke formation from hydrocarbons and oxygenates participate. Considering the fact that *I* coke is associated to more developed or graphitic type of carbonaceous residue, whose location lays on the meso and macropores of the FCC catalytic matrix, the *I*/*S* ratio shown in Table 6 demonstrates that the coke deposited on the VGO spent catalyst is located along the meso and macropores whereas that deposited on the RBO spent catalyst has a higher contribution of the coke located inside the micropores.

The results presented here enable to establish important synergies between the mechanisms of cracking-deactivation of hydrocarbons and oxygenates with competing adsorption of species on the acid sites (related to soluble coke). The predominant deposition pathway is that of heavy hydrocarbons present in the VGO fraction. The parallel hydride transfer reaction from hydrocarbons to oxygenates helps inhibiting the formation of coke from bio-oil oxygenates [59], and additionally, steam coming from RBO helps inhibiting the formation of insoluble coke from of the VGO. The predominance of the condensation reactions of bio-oil phenolic oxygenates forming coke (oxygenate deactivation pathway) has been proved before [51]. However, this predominance depends on the reaction conditions, particularly temperature. This explains the divergence of results in terms of catalyst deactivation when

bio-oil is present in the FCC unit, in general enhancing such deactivation [33,55]. Nevertheless, at temperatures higher than 500 °C the cracking of coke precursors or oligomers is quite effective [60], contributing to attenuate the oxygenate deactivation pathway. Besides, our results also show good perspectives of co-feeding bio-oil (in a moderate content in the feed) together with VGO in the FCC unit, and this does not cause additional problems in terms of catalyst deactivation. Indeed, steam contained in the RBO attenuates catalyst deactivation by means of stripping of coke precursors or competitive adsorption of these with steam, and this effect is more important than the cracking rate attenuation.

5. Conclusions

There are two mechanism of catalyst deactivation when co-feeding RBO and VGO, one of RBO yielding soluble and insoluble coke with relatively high proportion of H and O, the other one involves the deposition of coke with much higher aromaticity, formed through condensation of heavy molecules in the VGO in the meso and macropores of the catalyst. In both cases, coke deposited outside the zeolite blocks the accessibility of reactants to the acid sites. The existence of these mechanisms in the cracking of the blend creates synergetic effects with lower coke deposition compared with their constituents (VGO or RBO), what we interpreted due to the presence of steam in the RBO, that significantly decrease VGO coke deposition path. At the same time, VGO hydrocarbons act as hydrogen donors to RBO oxygenates, inhibiting the RBO coke deactivation path.

Coke deposited on the cracking of VGO is more aromatic, heavier, less soluble in CH_2Cl_2 and with bigger and highly ordered carbonaceous domains. Coke deposited in the cracking of RBO is more hydrogenated, oxygenated, lighter, more soluble in CH_2Cl_2 and with smaller highly-disordered carbonaceous domains. Coke deposited on the cracking of the blend has an intermediate composition between their components but its amount of insoluble coke is lower and has similar composition of that of the VGO spent catalyst, what has been rationalized as a lower deposition of the VGO heavy aromatics due to the presence of steam (from the RBO fraction). The relatively high temperature employed in the FCC unit, homogenizes the composition of coke despite the dominant VGO or RBO deactivation pathway.

Acknowledgements

The founding sources acknowledged for this work are the following: Ministry of Economy and Competitively of the Spanish Government (MINECO), cofounded with EFDR funds (projects CTQ2009-12800, CTQ2012-35192 and CTQ2013-46172-P), Basque Government (project IT748-13) and University of the Basque Country (UPV/EHU) (project UFI 11/39). Alvaro Ibarra is grateful for his PhD grant (BES-2010-032184). Authors also acknowledge Petronor S.A. and Ikerlan/IK-4 for providing with the feeds used in this work.

References

[1] A. Demirbas, Progress and recent trends in biofuels, Prog. Energy Combust. Sci. 33 (2007) 1–18.
[2] E. Butler, G. Devlin, D. Meier, K. McDonnell, A review of recent laboratory research and commercial developments in fast pyrolysis and upgrading, Renew. Sust. Energy Rev. 15 (2011) 4171–4186.
[3] A.V. Bridgwater, Review of fast pyrolysis of biomass and product upgrading, Biomass Bioenergy 38 (2012) 68–94.
[4] W.N.R.W. Isahak, M.W.M. Hisham, M.A. Yarmo, T.Y. Yun Hin, A review on bio-oil production from biomass by using pyrolysis method, Renew. Sust. Energy Rev. 16 (2012) 5910–5923.
[5] D. Meier, B. Van De Beld, A.V. Bridgwater, D.C. Elliott, A. Oasmaa, F. Preto, State-of-the-art of fast pyrolysis in IEA bioenergy member countries, Renew. Sust. Energy Rev. 20 (2013) 619–641.
[6] A. Oasmaa, B. Van De Beld, P. Saari, D.C. Elliott, Y. Solantausta, Norms, standards, and legislation for fast pyrolysis bio-oils from lignocellulosic biomass, Energy Fuels 29 (2015) 2471–2484.
[7] S. Czernik, A.V. Bridgwater, Overview of applications of biomass fast pyrolysis oil, Energy Fuels 18 (2004) 590–598.
[8] P.M. Mortensen, J.D. Grunwaldt, P.A. Jensen, K.G. Knudsen, A.D. Jensen, A review of catalytic upgrading of bio-oil to engine fuels, Appl. Catal. A: Gen. 407 (2011) 1–19.
[9] D. Carpenter, T.L. Westover, S. Czernik, W. Jablonski, Biomass feedstocks for renewable fuel production: a review of the impacts of feedstock and pretreatment on the yield and product distribution of fast pyrolysis bio-oils and vapors, Green Chem. 16 (2014) 384–406.
[10] A. Oasmaa, Y. Solantausta, V. Arpiainen, E. Kuoppala, K. Sipilä, Fast pyrolysis bio-oils from wood and agricultural residues, Energy Fuels 24 (2010) 1380–1388.
[11] G. Fogassy, N. Thegarid, Y. Schuurman, C. Mirodatos, The fate of bio-carbon in FCC co-processing products, Green Chem. 14 (2012) 1367–1371.
[12] A. Corma, L. Sauvanaud, FCC testing at bench scale: new units, new processes, new feeds, Catal. Today 218–219 (2013) 107–114.
[13] I. Graça, J.M. Lopes, H.S. Cerqueira, M.F. Ribeiro, Bio-oils upgrading for second generation biofuels, Ind. Eng. Chem. Res. 52 (2013) 275–287.
[14] M.S. Talmadge, R.M. Baldwin, M.J. Biddy, R.L. McCormick, G.T. Beckham, G.A. Ferguson, S. Czernik, K.A. Magrini-Bair, T.D. Foust, P.D. Metelski, C. Hetrick, M.R. Nimlos, A perspective on oxygenated species in the refinery integration of pyrolysis oil, Green Chem. 16 (2014) 407–453.
[15] D.V. Naik, V. Kumar, B. Prasad, B. Behera, N. Atheya, K.K. Singh, D.K. Adhikari, M.O. Garg, Catalytic cracking of pyrolysis oil oxygenates (aliphatic and aromatic) with vacuum gas oil and their characterization, Chem. Eng. Res. Des. 92 (2014) 1579–1590.
[16] M. Bertero, U. Sedran, Upgrading of bio-oils over equilibrium FCC catalysts. Contribution from alcohols, phenols and aromatic ethers, Catal. Today 212 (2013) 10–15.
[17] M. Bertero, G.D.L. Puente, U. Sedran, Products and coke from the conversion of bio-oil acids, esters, aldehydes and ketones over equilibrium FCC catalysts, Renew. Energy 60 (2013) 349–354.
[18] N. Thegarid, G. Fogassy, Y. Schuurman, C. Mirodatos, S. Stefanidis, E.F. Iliopoulou, K. Kalogiannis, A.A. Lappas, Second-generation biofuels by co-processing catalytic pyrolysis oil in FCC units, Appl. Catal. B: Environ. 145 (2014) 161–166.
[19] B. Valle, P. Castaño, M. Olazar, J. Bilbao, A.G. Gayubo, Deactivating species in the transformation of crude bio-oil with methanol into hydrocarbons on a HZSM-5 catalyst, J. Catal. 285 (2012) 304–314.
[20] M. Ibáñez, B. Valle, J. Bilbao, A.G. Gayubo, P. Castaño, Effect of operating conditions on the coke nature and HZSM-5 catalysts deactivation in the transformation of crude bio-oil into hydrocarbons, Catal. Today 195 (2012) 106–113.
[21] A. Ochoa, B. Aramburu, M. Ibáñez, B. Valle, J. Bilbao, A.G. Gayubo, P. Castaño, Compositional insights and valorization pathways for carbonaceous material deposited during bio-oil thermal treatment, ChemSusChem 7 (2014) 2597–2608.
[22] H.S. Cerqueira, G. Caeiro, L. Costa, F. Ramôa Ribeiro, Deactivation of FCC catalysts, J. Mol. Catal. A: Chem. 292 (2008) 1–13.
[23] M. Guisnet, P. Magnoux, Organic chemistry of coke formation, Appl. Catal. A: Gen. 212 (2001) 83–96.
[24] B. Valle, A.G. Gayubo, A. Alonso, A.T. Aguayo, J. Bilbao, Hydrothermally stable HZSM-5 zeolite catalysts for the transformation of crude bio-oil into hydrocarbons, Appl. Catal. B: Environ. 100 (2010) 318–327.
[25] R.S. Weber, M.V. Olarte, H. Wang, Modeling the kinetics of deactivation of catalysts during the upgrading of bio-oil, Energy Fuels 29 (2015) 273–277.
[26] G. Fogassy, N. Thegarid, Y. Schuurman, C. Mirodatos, From biomass to bio-gasoline by FCC co-processing: effect of feed composition and catalyst structure on product quality, Energy Environ. Sci. 4 (2011) 5068–5076.
[27] G. Fogassy, N. Thegarid, G. Toussaint, A.C. van Veen, Y. Schuurman, C. Mirodatos, Biomass derived feedstock co-processing with vacuum gas oil for second-generation fuel production in FCC units, Appl. Catal. B: Environ. 96 (2010) 476–485.
[28] L. Gueudré, N. Thegarid, L. Burel, B. Jouguet, F. Meunier, Y. Schuurman, C. Mirodatos, Coke chemistry under vacuum gasoil/bio-oil FCC co-processing conditions, Catal. Today 257 (2015) 200–214.
[29] J. Makibar, A.R. Fernandez-Akarregi, M. Amutio, G. Lopez, M. Olazar, Performance of a conical spouted bed pilot plant for bio-oil production by poplar flash pyrolysis, Fuel Process. Technol. 137 (2015) 283–289.
[30] H.I. De Lasa, Riser simulator, US Patent No. 5,102,628, 1992.
[31] F. Bauer, W.H. Chen, E. Bilz, A. Freyer, V. Sauerland, Surface modification of nano-sized HZSM-5 and HFER by pre-coking and silanization, J. Catal. 251 (2007) 258–270.
[32] A. Corma, S. Iborra, A. Velty, Chemical routes for the transformation of biomass into chemicals, Chem. Rev. 107 (2007) 2411–2502.
[33] A. Corma, G.W. Huber, L. Sauvanaud, P. O'Connor, Processing biomass-derived oxygenates in the oil refinery: catalytic cracking (FCC) reaction pathways and role of catalyst, J. Catal. 247 (2007) 307–327.
[34] F. De Miguel Mercader, M.J. Groeneveld, S.R.A. Kersten, N.W.J. Way, C.J. Schaverien, J.A. Hogendoorn, Production of advanced biofuels: co-processing of upgraded pyrolysis oil in standard refinery units, Appl. Catal. B: Environ. 96 (2010) 57–66.

[35] I. Graça, J.D. Comparot, S. Laforge, P. Magnoux, J.M. Lopes, M.F. Ribeiro, F.R. Ribeiro, Influence of phenol addition on the H-ZSM-5 zeolite catalytic properties during methylcyclohexane transformation, Energy Fuels 23 (2009) 4224–4230.
[36] I. Graça, J.D. Comparot, S. Laforge, P. Magnoux, J.M. Lopes, M.F. Ribeiro, F. Ramoa Ribeiro, Effect of phenol addition on the performances of H–Y zeolite during methylcyclohexane transformation, Appl. Catal. A: Gen. 353 (2009) 123–129.
[37] Y. Zhao, F. Wei, Y. Yu, Inhibition of coke formation in Cracking of 2-methylpentane on USHY by addition of steam, Chin. J. Chem. Eng. 16 (2008) 726–732.
[38] L. Nie, D.E. Resasco, Improving carbon retention in biomass conversion by alkylation of phenolics with small oxygenates, Appl. Catal. A: Gen. 447–448 (2012) 14–21.
[39] A.T. To, D.E. Resasco, Hydride transfer between a phenolic surface pool and reactant paraffins in the catalytic cracking of m-cresol/hexanes mixtures over an HY zeolite, J. Catal. 329 (2015) 57–68.
[40] A.T. Aguayo, P. Castaño, D. Mier, A.G. Gayubo, M. Olazar, J. Bilbao, Effect of cofeeding butane with methanol on the deactivation by coke of a HZSM-5 zeolite catalyst, Ind. Eng. Chem. Res. 50 (2011) 9980–9988.
[41] P. Castaño, G. Elordi, M. Olazar, J. Bilbao, Imaging the profiles of deactivating species on the catalyst used for the cracking of waste polyethylene by combined microscopies, ChemCatChem 4 (2012) 631–635.
[42] F. Bauer, H.G. Karge, Characterization of coke on zeolites, Mol. Sieves 5 (2007) 249–364.
[43] H.S. Cerqueira, C. Sievers, G. Joly, P. Magnoux, J.A. Lercher, Multitechnique characterization of coke produced during commercial resid FCC Operation, Ind. Eng. Chem. Res. 44 (2005) 2069–2077.
[44] P. Magnoux, H.S. Cerqueira, M. Guisnet, Evolution of coke composition during ageing under nitrogen, Appl. Catal. A: Gen. 235 (2002) 93–99.
[45] A.T. Aguayo, A.G. Gayubo, J. Ereña, A. Atutxa, J. Bilbao, Coke aging and its incidence on catalyst regeneration, Ind. Eng. Chem. Res. 42 (2003) 3914–3921.
[46] J.L. Bonardet, M.C. Barrage, J. Fraissard, Use of NMR techniques for studying deactivation of zeolites by coking, J. Mol. Catal. A: Chem. 96 (1995) 123–143.
[47] A.C. Ferrari, Raman spectroscopy of graphene and graphite: disorder, electron-phonon coupling, doping and nonadiabatic effects, Solid State Commun. 143 (2007) 47–57.
[48] B. Guichard, M. Roy-Auberger, E. Devers, B. Rebours, A.A. Quoineaud, M. Digne, Characterization of aged hydrotreating catalysts. Part I: coke depositions, study on the chemical nature and environment, Appl. Catal. A: Gen. 367 (2009) 1–8.
[49] M. Ibáñez, M. Artetxe, G. Lopez, G. Elordi, J. Bilbao, M. Olazar, P. Castaño, Identification of the coke deposited on an HZSM-5 zeolite catalyst during the sequenced pyrolysis–cracking of HDPE, Appl. Catal. B: Environ. 148–149 (2014) 436–445.
[50] P. Magnoux, P. Roger, C. Canaff, V. Fouche, N.S. Gnep, M. Guisnet, New technique for the characterization of carbonaceous compounds responsible for zeolite deactivation, Stud. Surf. Sci. Catal. 34 (1987) 317–330.
[51] L. Pinard, S. Hamieh, C. Canaff, F. Ferreira Madeira, I. Batonneau-Gener, S. Maury, O. Delpoux, K. Ben Tayeb, Y. Pouilloux, H. Vezin, Growth mechanism of coke on HBEA zeolite during ethanol transformation, J. Catal. 299 (2013) 284–297.
[52] A. Feller, J.O. Barth, A. Guzman, I. Zuazo, J.A. Lercher, Deactivation pathways in zeolite-catalyzed isobutane/butene alkylation, J. Catal. 220 (2003) 192–206.
[53] J.L. Fernandes, L.H. Domingues, C.I.C. Pinheiro, N.M.C. Oliveira, F.R. Ribeiro, Influence of different catalyst deactivation models in a validated simulator of an industrial UOP FCC unit with high-efficiency regenerator, Fuel 97 (2012) 97–108.
[54] A.G. Gayubo, B. Valle, A.T. Aguayo, M. Olazar, J. Bilbao, Attenuation of catalyst deactivation by cofeeding methanol for enhancing the valorisation of crude bio-oil, Energy Fuels 23 (2009) 4129–4136.
[55] H. Zhang, Y.T. Cheng, T.P. Vispute, R. Xiao, G.W. Huber, Catalytic conversion of biomass-derived feedstocks into olefins and aromatics with ZSM-5: the hydrogen to carbon effective ratio, Energy Environ. Sci. 4 (2011) 2297–2307.
[56] Y.G. Adewuyi, D.J. Klocke, J.S. Buchanan, Effects of high-level additions of ZSM-5 to a fluid catalytic cracking (FCC) RE-USY catalyst, Appl. Catal. A: Gen. 131 (1995) 121–133.
[57] J.M. Arandes, I. Torre, M.J. Azkoiti, P. Castaño, J. Bilbao, H. de Lasa, Effect of catalyst properties on the cracking of polypropylene pyrolysis waxes under FCC conditions, Catal. Today 133 (2008) 413–419.
[58] J.M. Arandes, I. Torre, P. Castaño, M. Olazar, J. Bilbao, Catalytic cracking of waxes produced by the fast pyrolysis of polyolefins, Energy Fuels 21 (2007) 561–569.
[59] V.P. Doronin, O.V. Potapenko, P.V. Lipin, T.P. Sorokina, Catalytic cracking of vegetable oils and vacuum gas oil, Fuel 106 (2013) 757–765.
[60] S. Li, S. Zhang, Z. Feng, Y. Yan, Characterization of the coke in the coprocessing of bio-oil with paraffin oil, Environ. Progress Sust. Energy 33 (2014) 1373–1379.